Geophysical Journal International

Geophys. J. Int. (2020) **220,** 296–307
Advance Access publication 2019 October 10
GJI Seismology

doi: 10.1093/gji/ggz408

Marchenko methods in a 3-D world

A. Lomas [1] and A. Curtis[1,2]

[1] *School of GeoSciences, University of Edinburgh, Edinburgh, EH9 3FE, UK. E-mail: angus.lomas@ed.ac.uk*
[2] *Institute of Geophysics, ETH Zurich,* 8092 *Zurich, Switzerland*

Accepted 2019 October 8. Received 2019 July 28; in original form 2018 October 15

SUMMARY

Marchenko methods are a suite of geophysical techniques that convert seismograms of energy created by surface sources and measured by surface receivers into seismograms that would have been recorded by a virtual receiver at an arbitrary point inside the subsurface—an operation called redatuming. In principle these redatumed seismograms contain all contributions from direct, primary (singly-reflected) and multiply-reflected waves that would have been recorded by a real subsurface receiver, without requiring prior information about interfaces that generated the reflections. The potential of these methods for seismic imaging and redatuming has been demonstrated extensively in previous literature, but only using 1-D and 2-D Marchenko methods. There remain aspects of the methods that are poorly understood when applied in a 3-D world, so we investigate the application of Marchenko methods to 3-D data, subsurface structures and wavefields. We first show that for waves propagating in three dimensions, Marchenko methods can be applied to seismic data collected using both linear (so-called 2-D seismic) and areal (3-D seismic) acquisition arrays. However, for 2-D acquisition arrays the Marchenko workflow requires additional dimensionality correction factors to obtain accurate solutions, even in a subsurface that only varies with depth. Without these correction factors phase errors occur in redatumed Marchenko estimates; these errors propagate through the Marchenko algorithm and create depth errors in the Marchenko images. Furthermore, applying Marchenko methods to fully 3-D seismic wavefields recorded by linear (2-D seismic) arrays that contain out-of-plane reflections deteriorates surface-to-subsurface Green's function estimates with spurious energy and resulting images are less accurate than those created using 'conventional' imaging methods. The application of fully 3-D Marchenko methods using data recorded on areal arrays solves both of the above problems, creating accurately redatumed wavefields and images with reduced artefact contamination. However, it appears that source–receiver spacing at most of $\lambda_A/4$ is required for accurate results using existing Marchenko methods, where λ_A is the dominant wavelength and in many real 3-D seismic acquisition scenarios this is impractical.

Key words: Controlled source seismology; Wave propagation; Wave scattering and diffraction.

1 INTRODUCTION

The aim of seismic imaging is to produce maps indicative of spatial variations in properties of the Earth's subsurface. Methods of seismic imaging, such as Reverse Time Migration (RTM – Baysal *et al.* 1983) typically use seismograms recorded on or near the surface of the Earth and assume that seismic reflections observed in these seismograms are singly-scattered, meaning that they have reflected or diffracted only once from subsurface heterogeneities. This assumption is imposed within such methods by the use of a low-wavenumber, smoothly varying estimate of the subsurface seismic velocity, to extrapolate surface seismic data into the subsurface. Extrapolating the injected source wavefield estimates what the wavefield looked like before it scattered, and back-extrapolating the wavefield recorded at the surface estimates the subsurface wavefield after it scattered (both operations being called redatuming). These wavefield are combined to form an image of any scattering heterogeneity that converted the source wavefield into the receiver wavefield. However, the extrapolated wavefields and hence the images are generally in error since in reality some parts of the

wavefield scattered multiple times from the omitted high wavenumber velocity variations as they propagate through the subsurface.

Marchenko methods overcome the single scattering assumption by extrapolating wavefields into the subsurface including all multiply-scattered waves, even when only a smoothly varying estimate of the subsurface velocity structure is available (Broggini *et al.* 2012; Wapenaar *et al.* 2013). Images created using these wavefields and a variety of imaging conditions exhibit a reduction in the artefacts that usually contaminate seismic images due to multiples (da Costa Filho *et al.* 2015; da Costa Filho & Curtis 2016; Singh & Snieder 2017).

Following the development of Marchenko methods (Marchenko 1955; Rose 2001; Broggini *et al.* 2012) their application was initially limited to synthetic acoustic seismic imaging and redatuming problems without allowing for free-surface reflections (Wapenaar *et al.* 2013). Further developments have extended Marchenko methods to elastic media (da Costa Filho *et al.* 2014, 2015 Wapenaar 2014) and to seismic data containing free surface multiples (Singh *et al.* 2015, 2016). More recently Marchenko methods have been applied to real, reservoir scale, seismic data sets (Ravasi *et al.* 2016; Jia *et al.* 2017; Staring *et al.* 2018) and to real ultrasonic data (Cui *et al.* 2018a; da Costa Filho *et al.* 2018; Wapenaar *et al.* 2018). However, given the novelty of these methods there are still aspects that are poorly understood. One of these, and the focus of this paper, is the behaviour of Marchenko methods when applied to 3-D seismic data, structures and wavefields.

Marchenko methods are based on mathematical derivations by Wapenaar *et al.* (2013) that all assume three spatial dimensions, but only recently have Marchenko methods been applied to 3-D seismic data (Lomas & Curtis 2017). The prospect of applying Marchenko methods in three dimensions was discussed in earlier work (Wapenaar *et al.* 2014), however concerns were raised about the practicalities of the spatially dense acquisition geometries that would be required for the input reflectivity. This is because similarly to seismic interferometry (Snieder 2004a; Curtis *et al.* 2006) and RTM (Baysal *et al.* 1983), Marchenko methods rely on destructive and constructive interference of seismograms from neighbouring source and receivers in order to produce the seismograms of interest. Recorded waveforms can only accurately interact with adjacent signals if they are recorded with a source or receiver spacing that is a fraction of the seismic wavelength (van Manen *et al.* 2005, 2006; Wapenaar & Fokkema 2006), hence the concern.

In this paper, we first show that Marchenko methods hold in three dimensions when seismic data collected with sufficient boundary coverage in both horizontal directions are available. However, given issues with the practicality of acquiring such data we also assess the performance of Marchenko methods on data acquired along a linear surface seismic array above a 3-D Earth. We show that simply subsampling the full areal 3-D wavefield along this line and applying the same Marchenko methods produces a redatumed wavefield that contains phase inconsistencies which produce depth errors in subsurface images. These can be removed by the application of correction factors within the Marchenko workflow to account for inconsistencies in dimensionality. Finally, we demonstrate the impact of out-of-plane reflections on Marchenko estimates using data from linear seismic arrays. We show that these can be detrimental to the redatumed seismograms and the resulting images. These errors do not exist when using seismic data from full areal arrays.

2 MARCHENKO METHODS

2.1 Theory

The theoretical foundations of Marchenko methods are the one-way reciprocity theorems of the convolution and correlation type for pressure-normalized wavefields (Wapenaar & Grimbergen 1996; Wapenaar *et al.* 2014):

$$-\int_{\partial\mathbb{D}_0}\rho^{-1}\left[p_A^+(\partial_z p_B^-)+p_A^-(\partial_z p_B^+)\right]\,d^2\mathbf{x}_0 = \int_{\partial\mathbb{D}_i}\rho^{-1}\left[(\partial_z p_A^+)p_B^- + (\partial_z p_A^-)p_B^+\right]\,d^2\mathbf{x}_i \quad (1)$$

$$-\int_{\partial\mathbb{D}_0}\rho^{-1}\left[p_A^{+*}(\partial_z p_B^+)+p_A^{-*}(\partial_z p_B^-)\right]\,d^2\mathbf{x}_0 = \int_{\partial\mathbb{D}_i}\rho^{-1}\left[(\partial_z p_A^+)^* p_B^+ + (\partial_z p_A^-)^* p_B^-\right]\,d^2\mathbf{x}_i. \quad (2)$$

Eqs (1) and (2) are the 3-D acoustic reciprocity theorems given in the frequency domain. Two states are represented by A and B, and these represent directionally decomposed $(+/-)$ wavefields (p) travelling through two different media (or subsurface models) chosen to be those described in Fig. 1. These wavefields are decomposed to represent either the component propagating downwards $(+)$ or upwards $(-)$ at the recording location, therefore no horizontally propagating waves are accounted for within current Marchenko theory. Eqs (1) and (2) describe the relationship between the measured wavefields in these two different media. We define state A to be a so-called focusing state, in which the wavefield injected at the surface would focus to create a spatio-temporal impulse at location $\mathbf{x}_i' = (x', y', i)$ at time defined to be $t = 0$. Thereafter this impulsive energy will diverge like a source placed at $\mathbf{x}_i'$. In order for this to be possible the medium is defined to be equal to the true Earth's acoustic structure above, and to be reflection-free below the horizontal subsurface boundary $\partial\mathbb{D}_i$; this defines the so-called reference medium. State B is the true medium within which the true Green's functions between the surface source–receiver array at locations $\mathbf{x}_0''/\mathbf{x}_0$ (on the horizontal surface boundary $\partial\mathbb{D}_0$) and the subsurface point $\mathbf{x}_i'$ exist, and these are ultimately the wavefields of interest. We define Green's functions (G) as the pressure recordings measured at a receiver location due to the firing of a spatio-temporally impulsive source at $t = 0$: G therefore depends on source and receiver locations and on frequency or time. Additionally, $\mathbf{x}_0$ represents an array of points with a fixed depth coordinate $z = 0$ and a variable horizontal coordinate at an array of locations which vary in both the first (x) and second (y) horizontal dimension: $\mathbf{x}_0 = \{(x_j, y_j, 0) : j = 1, 2, \ldots, N\}$, where N is the number of surface source–receiver positions. For the implementation presented here $\mathbf{x}_0$ has to equal $\mathbf{x}_0''$ and $\mathbf{x}_i'$ represents a point on the boundary $\partial\mathbb{D}_i$.

Given the relationships described in Fig. 1 we can assign values to the wavefields of interest in eqs (1) and (2). In state B quantity $p_B^{+/-}$ is a Green's function created by a source at location $\mathbf{x}_0''$ and measured on the boundary represented by the integral ($\partial\mathbb{D}_{0/i}$). In state A, quantity $p_A^{+/-}$ is a focusing function (denoted $f^{+/-}$ below). We define a downgoing focusing function f^+ as a set of signals that when injected at a boundary as a source time function would collapse to a singular peak in the pressure field at the focusing location; the upgoing focusing function f^- is the reflected component (in State A) of the downing focusing function recorded at the injection surface. In state A we define the focusing location as a point $\mathbf{x}_i'$ on the boundary $\partial\mathbb{D}_i$. This focus is created by injecting a source time

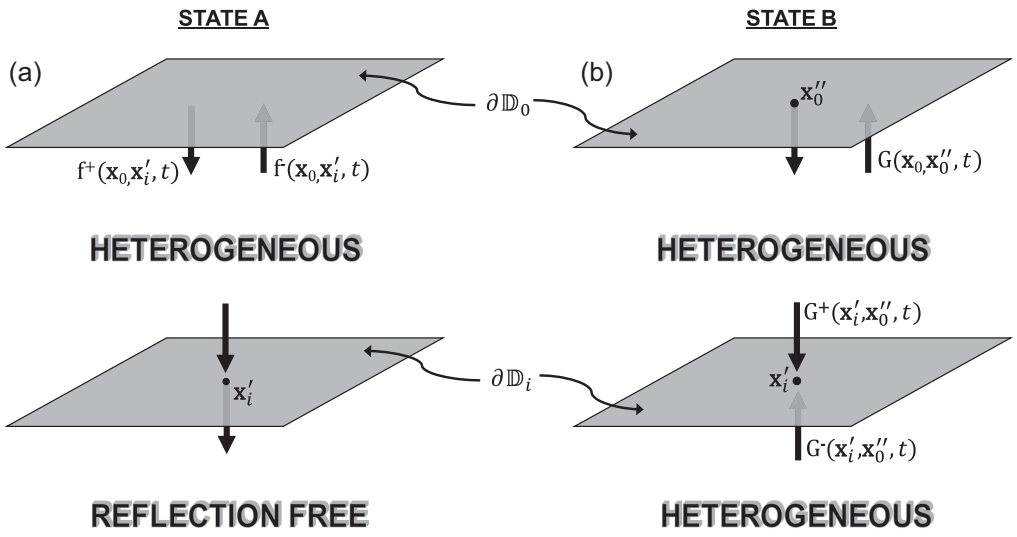

Figure 1. A 3-D diagrammatic comparison of the differences between states A and B, described in eqs (1) and (2). Panel (a) shows state A (the reference medium) which is equal to the true medium above constant depth boundary $\partial\mathbb{D}_i$, and is reflection free below $\partial\mathbb{D}_i$ where $\mathbf{x}_i$ is the focusing location and is a point on the boundary $\partial\mathbb{D}_i$. Panel (b) is the true medium, which is identical to state A above the surface $\partial\mathbb{D}_i$ but also includes the true medium heterogeneity below this depth.

function at the boundary represented by the integral ($\partial\mathbb{D}_{0/i}$). Hence the values are defined as $p_A^{+/-} = f^{+/-}(\mathbf{x}_0/\mathbf{x}_i, \mathbf{x}_i', \omega)$ and $p_B^{+/-} = G^{+/-}(\mathbf{x}_0/\mathbf{x}_i, \mathbf{x}_0'', \omega)$. We assume free-surface multiples have been removed from the data so that the upper (ground surface) boundary $\partial\mathbb{D}_0$ is effectively absorbing. Furthermore, state A is reflection free below the boundary $\partial\mathbb{D}_i$. These two conditions allow us to simplify eqs (1) and (2) when we substitute in the wavefields defined above—this is formally derived in appendix A of Wapenaar *et al.* (2014), and fully expanded this gives:

$$G^-(x,y,i;x'',y'',0;\omega) = \iint_{\partial\mathbb{D}_0}[R(x'',y'',0;x,y,0;\omega) \times f^+(x,y,0;x,y,i;\omega)]\mathrm{d}x\,\mathrm{d}y - f^-(x'',y'',0;x,y,i;\omega) \quad (3)$$

$$G^+(x,y,i;x'',y'',0;\omega) = f^+(x'',y'',0;x,y,i;\omega)^* - \iint_{\partial\mathbb{D}_0}[R(x'',y'',0;x,y,0;\omega) f^-(x,y,0;x,y,i;\omega)^*]\mathrm{d}x\,\mathrm{d}y. \quad (4)$$

Eqs (3) and (4) are the 3-D equivalent of eqs (11) and (12) presented by Wapenaar *et al.* (2014) (as well as most of the literature on this topic), therefore for convenience we will revert back to standard notation from this point forward, where $\mathbf{x}_i = (x', y', i)$, $\mathbf{x}_0 = (x, y, 0)$ and $\mathbf{x}_0'' = (x'', y'', 0)$. Eqs (3) and (4) define a relationship in three dimensions between the focusing functions (f) and the Green's functions (G) of interest. These are linked by the reflectivity (R) which is the vertical (z) particle velocity component measured in the true medium and created by a volume injection rate impulsive source, where both the sources and receivers are on the boundary $\partial\mathbb{D}_0$ (Wapenaar & Fokkema 2006). Additionally this is multiplied by a scaling factor of -2 and by reciprocity is equivalent to the pressure recording but created by a vertical force source (Thorbecke *et al.* 2017).

The aim of the Marchenko method is to calculate the Green's functions. However, the only known quantity in eqs (3) and (4) is the measured reflectivity. Therefore, to solve for G^+ and G^- we require a method that enables an estimate of the focusing functions to be obtained. An elegant algorithmic way to solve this problem is first described by Slob *et al.* (2014) and Wapenaar *et al.* (2014), discussions of the mathematical foundation of the algorithm are described by van der Neut *et al.* (2015a), and an intuitive demonstration of how this method works is given by van der Neut *et al.* (2015c), Cui *et al.* (2018b) and Lomas & Curtis (2019). The algorithm is an iterative procedure which requires as input both an estimate of the reflectivity (R), and an estimate of the direct arrival between the chosen virtual receiver (location $\mathbf{x}_i$) and the surface sources (denoted T_d). The algorithm is embodied within eqs (5)–(8), and upon convergence the solutions for $f^{+/-}$ can be used as input to eqs (3) and (4):

$$f_0^-(\mathbf{x}_0'',\mathbf{x}_i',\omega) \approx \theta \int_{\partial\mathbb{D}_0}\left[R(\mathbf{x}_0'',\mathbf{x}_0,\omega)T_d(\mathbf{x}_0,\mathbf{x}_i',\omega)^*\right]d^2\mathbf{x}_0 \quad (5)$$

$$M_n^+(\mathbf{x}_0'',\mathbf{x}_i',\omega)^* = \theta \int_{\partial\mathbb{D}_0}\left[R(\mathbf{x}_0'',\mathbf{x}_0,\omega)f_{n-1}^-(\mathbf{x}_0,\mathbf{x}_i',\omega)^*\right]d^2\mathbf{x}_0 \quad (6)$$

$$f_n^-(\mathbf{x}_0'',\mathbf{x}_i',\omega) = f_0^-(\mathbf{x}_0'',\mathbf{x}_i',\omega) + \theta \int_{\partial\mathbb{D}_0}\left[R(\mathbf{x}_0'',\mathbf{x}_0,\omega) \times M_n^+(\mathbf{x}_0,\mathbf{x}_i',\omega)\right]d^2\mathbf{x}_0 \quad (7)$$

$$f_n^+(\mathbf{x}_0'',\mathbf{x}_i',\omega) \approx T_d(\mathbf{x}_i',\mathbf{x}_0'',\omega)^* + M_n^+(\mathbf{x}_0'',\mathbf{x}_i',\omega). \quad (8)$$

In eq. (5), the complex conjugate (*) of the estimated direct arrival (T_d) in the frequency domain (ω) is convolved with the reflectivity (a multiplication in the frequency domain). The result is multiplied by a window $\theta(\mathbf{x}_0'',\mathbf{x}_i',t)$ in the time domain which filters out data that does not contribute to the focusing functions. The operator θ is therefore defined as a transform from the frequency to the time domain, a multiplication by window θ and then a transfer from the time to the frequency domain. The time window component of this

operation is defined as:

$$\theta(\mathbf{x}_0'', \mathbf{x}_i', t) = \begin{cases} 0 & t \leq -t_d(\mathbf{x}_0'', \mathbf{x}_i') \\ 1 & -t_d(\mathbf{x}_0'', \mathbf{x}_i') < t < t_d(\mathbf{x}_0'', \mathbf{x}_i') \\ 0 & t \geq t_d(\mathbf{x}_0'', \mathbf{x}_i'), \end{cases} \tag{9}$$

where t_d is the traveltime between its two arguments ($\mathbf{x}_0''$ and $\mathbf{x}_i'$). The initial estimate for f_0^- is then used to begin a procedure that iterates eqs (6) and (7). These two equations are repeated for n iterations, until convergence, upon which eq. (7) produces a value for the upgoing focusing function f^- and eq. (6) produces a value for the coda (scattered component) of the downgoing focusing function M_n^+. The final step consists of solving for f_n^+ by summing T_d and M_n^+ (eq. 8).

Eqs (3)–(8) are the 3-D form of the 2-D equations implemented in existing applications of the Marchenko method. The only difference between the two forms is the acquisition boundary which has changed from a line in 2-D applications to a surface integral in 3-D applications, and consequently an extra dimension is added to all coordinates.

2.2 Dimensionality of seismic data

There are two main factors to consider when working with 3-D rather than 2-D wavefields. The first is the difference between measured responses to waves propagating through 2-D and 3-D media. The second is the data acquisition array, given that the Marchenko method ideally needs full boundary coverage (to infinite offsets) in both horizontal spatial dimensions to perform integrals in the equations above.

First consider the measured seismic response for a wavefield propagating through a lossless 3-D medium. In this case a source signal will propagate outwards from the injection point in all directions (x, y, z) distributing the initial energy over an increasingly large wavefront as it propagates. This change in energy is a function of the distance any packet of energy on the wavefield has travelled $r = |\mathbf{x}_i' - \mathbf{x}_0''|$. In three dimensions this energy change is proportional to the surface area of a sphere, hence the amplitude change is a function of $1/r$ (since amplitude is proportional to the square root of the energy). In two dimensions the same intuition applies but the energy is only distributed over a 2-D wavefront (x, z) so amplitude change is instead a function of $1/\sqrt{r}$. Furthermore, differences in phase, and an additional frequency dependent difference in amplitude occur between two and three dimensions. These various differences can be expressed mathematically within the expressions for the 2-D and 3-D Green's functions for a homogeneous medium as (Snieder 2004b; Auer *et al.* 2013; Galetti *et al.* 2013):

$$G^{2D}(r, k) \approx \frac{1}{2\sqrt{2\pi kr}} \exp\left(ikr + \frac{i\pi}{4}\right) \tag{10}$$

$$G^{3D}(r, k) = \frac{1}{4\pi r} \exp(ikr). \tag{11}$$

Eqs (10) and (11) are expressed in the frequency domain. However, for simplicity of notation we have expressed the solutions in terms of angular wavenumber k, which is a function of angular frequency (ω) and the velocity (c) of the medium ($k = \frac{\omega}{c}$). It is worth noting that the 2-D Green's function (G^{2D}) given in eq. (10) is an approximate solution which is valid in the far-field of the source. This approximation only holds if the distance r is significantly greater than the wavelength ($r > \lambda$).

Given the formula in eqs (10) and (11) we can calculate an approximate function that transforms data from waves propagating in a first dimensionality into the equivalent data that would have been obtained if the waves had propagated in the other dimensionality:

$$G^{2D}(r, k) \approx G^{3D}(r, k)\sqrt{\frac{2\pi r}{k}} \exp\left(\frac{i\pi}{4}\right) \tag{12}$$

$$G^{3D}(r, k) \approx G^{2D}(r, k)\sqrt{\frac{k}{2\pi r}} \exp\left(-\frac{i\pi}{4}\right). \tag{13}$$

Implementing the filters in eqs (12) and (13) is not straightforward in variable velocity media because the ray path r is generally unknown. Implementation is therefore often approximated (Auer *et al.* 2013) or r can be estimated using ray theory (Bleistein 1986). In this paper this problem has been avoided by using a known constant velocity medium but we acknowledge that in further work in variable-velocity media a more robust algorithm will be required and there will be errors associated with our implementation.

In Fig. 2, we have modelled wave propagation using staggered-grid finite difference methods through a 2-D and a 3-D medium (G_{TRUE}). The measured responses for a set of source–receiver pairs at an offset of 750 m are plotted in black in Figs 2(a) and (b). In this example the injected wavelet is the temporal derivative of a 15 Hz Ricker wavelet. Each of these two signals is then transformed to the other dimensionality to test the accuracy of the transfer functions given in eqs (12) and (13), with results given by the dashed red lines in Figs 2(a) and (b).

Fig. 2 confirms, perhaps counter intuitively that the response to a Ricker wavelet source in two dimensions is more complex than it is in three dimensions, undergoing a phase shift which offsets the zero-crossing from the predicted arrival time (marked by a black cross). The comparisons after transferring between the two forms of Green's function are a good match even though this is not an exact solution given the approximation made in eq. (10) and errors in the finite difference wave propagation. These transforms will therefore be used in the remainder of this paper. It is important to consider these differences when implementing the Marchenko method in three dimensions. All real data from seismic waveforms originates from 3-D wave propagation, however it is very common for seismic surveys to sample these wavefields only in two dimensions (e.g. seismic streamers use approximately linear spatial arrays plus time).

3 EXPERIMENTAL SETUP

The seismic data examples presented in this paper are based on a synthetic data set, created by modelling acoustic seismic wave propagation through a 3-D subsurface model. The model has variable density but a constant velocity (3000 m s^{-1}) in order to make straight ray based interpretations of the various packets of energy. It contains a 3-D trough structure, which varies in both the x and y directions, and multiple horizontal planar layers (see Fig. 3). Although this model is simple it was designed to optimize compute times due to its symmetries about vertical planes, to easily separate events observed in the seismic wavefield and to enable simple analysis of the results, yet to contain sufficient 3-D structure to illuminate features of interest.

The seismic data from each impulsive source at location $\mathbf{x}_0$ to all receivers at locations $\mathbf{x}_0''$ are used as an approximation to the 3-D reflectivity $R(\mathbf{x}_0'', \mathbf{x}_0, t)$, measured using an areal grid of sources and receivers on the model ground surface ($z = 0$). Sources and receivers are colocated at 32 m intervals in both directions giving a total of 5922 locations (Fig. 3b). This spacing was chosen to reduce the computational cost of Marchenko receiver redatuming but ensure

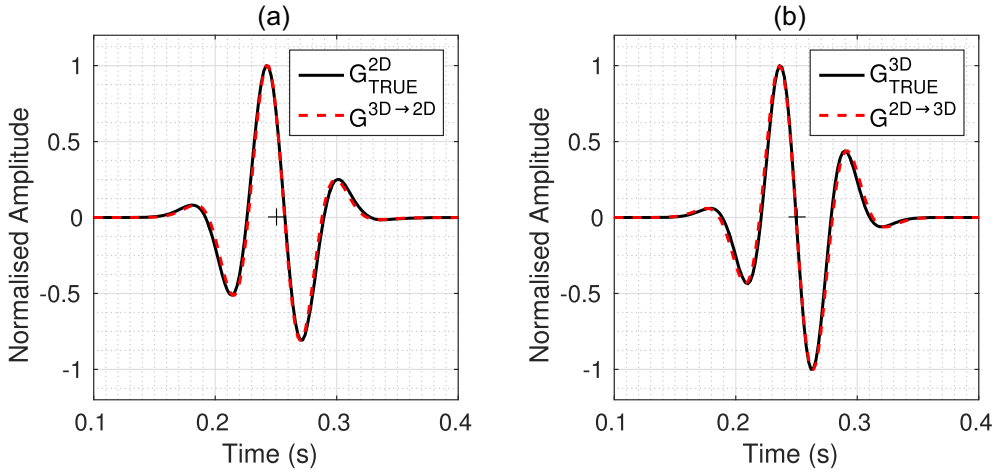

Figure 2. A comparison of the modelled responses following the injection of a 15Hz Ricker derivative wavelet inside a homogeneous medium ($c = 3000\,\mathrm{m\,s^{-1}}$). Panels (a) and (b) compare the signals that are measured at the receiver in two and three dimensions respectively in repose to a source of 750 m offset. A second comparison in panels (a) and (b) show the modelled 3-D Green's function converted to the equivalent 2-D Green's function (panel a) and the modelled 2-D Green's function converted to the equivalent 3-D Green's function (panel b).

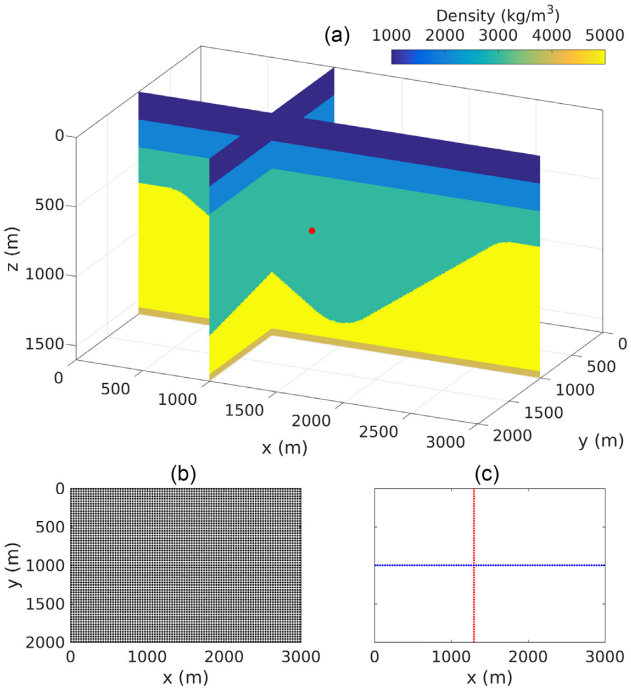

Figure 3. The 3-D variable density, constant velocity ($3000\,\mathrm{m\,s^{-1}}$) model used to created synthetic seismic data. In panel (a) we compare two slices through the model ($x = 1004$ m and $y = 1000$ m). The red sphere defines a subsurface virtual receiver position $\mathbf{x}_i$ at location at (1292 m, 1000 m, 600 m). Panels (b) and (c) show the areal and linear acquisition geometries used in later sections of this paper: each dot is both a source and receiver location. The linear arrays in panel (c) are at $x = 1292$ m and $y = 1000$ m.

accurate solutions were obtained. The source wavelet for the reflectivity is a constant-amplitude frequency spectrum wavelet with a bandwidth of 0−45 Hz, so designed to remove the need for source-signature deconvolution that would otherwise be required in order to estimate R, thus eliminating a potential source of error (Thorbecke *et al.* 2017). A second 15 Hz Ricker derivative wavelet, is used to calculate the direct arrival (eq. 5); as this is then convolved with the reflectivity, which has a flat frequency spectrum, this is the 'effective' injected wavelet that will be contained within our Marchenko Green's function estimates and in this example this was modelled to reduce errors in the estimated Green's function. We produced seismic data using the parameters described above, with each of the 5922 source positions measured by all 5922 receivers—a total of 35 070 084 seismic traces. Each of these traces has a recording length of 2 s and a temporal sampling interval of 0.002 s. These data form the reflectivity R used as input to the 3-D Marchenko algorithm (eqs 3–8).

In the later sections of this paper we consider the implications of subsampling the 3-D seismic data along spatially linear source and receiver arrays shown in Fig. 3(c). The reflectivity for these linear arrays are created by taking sources and receivers first with a constant y co-ordinate (blue profile) and then a constant x co-ordinate (red profile).

4 3-D GREEN'S FUNCTION ESTIMATION

We can use the seismic data set and the virtual receiver position defined in Fig. 3 as input to the 3-D Marchenko algorithm defined in eqs (3)–(8). First, five iterations of eqs (5)–(8) are used to estimate the focusing functions f_n^+ and f_n^- which are shown in Figs 4(a) and (b), respectively. Then we solve for the directionally decomposed Green's functions $G^{+/-}$ using eqs (3) and (4) and sum the result to obtain the full Green's function $G = G^+ + G^-$. This result can be compared to the true modelled Green's function as displayed in Fig. 4(d).

Qualitative analysis of Fig. 4 suggests a good match between the true and estimated Green's functions. A second test of the solution accuracy is given in Fig. 5(a) where we make a trace by trace comparison of the calculated 3-D Marchenko estimate and the modelled Green's function (recorded along a 2-D profile). The results demonstrate the applicability of Marchenko methods to 3-D wavefields and structures. There are some small discrepancies in Green's function components at far offsets due to the wavefields interacting with the steeply dipping trough structure (see Fig. 3). The poorer

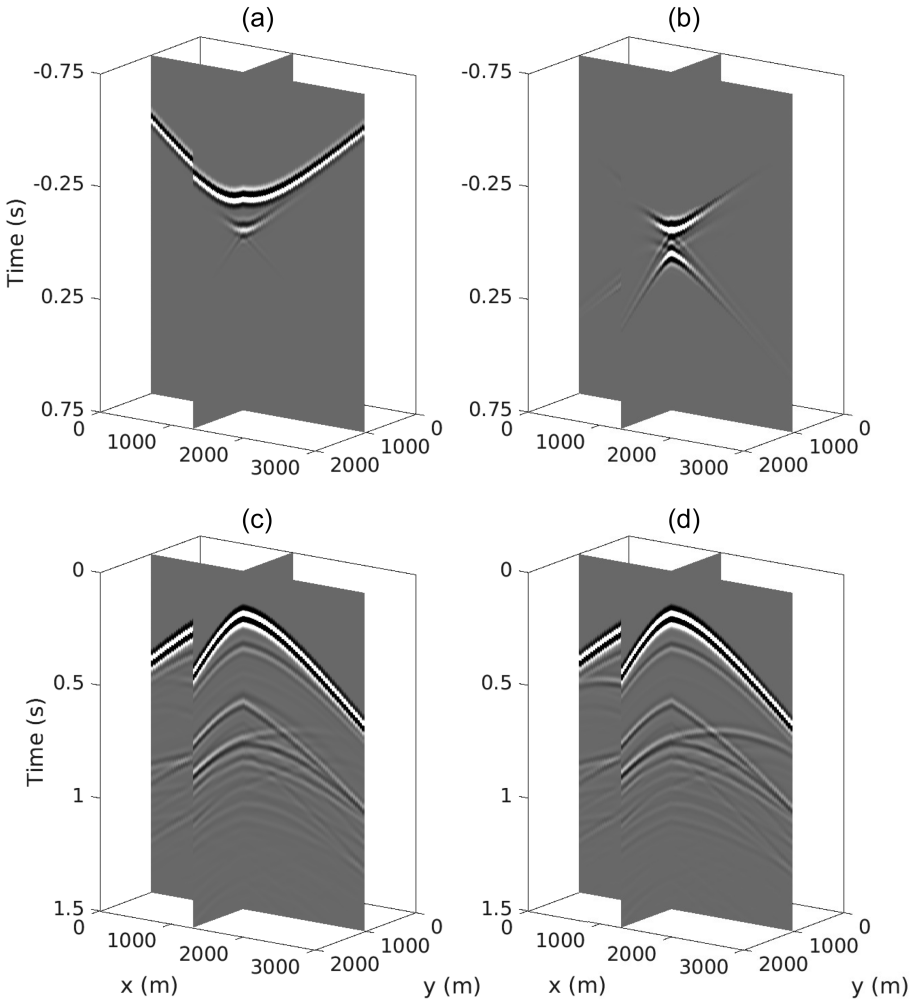

Figure 4. 3-D focusing functions, common virtual receiver gathers estimated using the Marchenko method, and directly modelled Green's functions. Panels (a) and (b) respectively show the estimated solutions for the focusing functions f_n^+ and f_n^- obtained from eqs (5) to (8). These functions are used to estimate the Green's functions $G = G^+ + G^-$ where $G^{+/-}$ are estimated from eqs (3) and (4), and G is displayed in panel (c). This can be compared to the directly modelled Green's functions in panel (d).

estimation of these components is due to the limited source and receiver aperture of the seismic array (the errors increase as aperture is decreased) and hence could be improved by including additional sources and receivers beyond the extremities of the current experiment. This limitation is not unique to this method and is also known to cause inaccuracies in conventional imaging algorithms like RTM.

A consideration for all implementations of Marchenko methods is how to scale the amplitude of the reflectivity. Marchenko methods will only iterate to accurate solutions when the amplitude of the true reflectivity is known. This problem is often overcome in synthetic experiments by using perfectly scaled wave propagation codes but in our experiment, as is the case with real seismic (field) data, the reflectivity is not scaled correctly. We therefore implement a method for calculating a scaling factor (which is then multiplied by the reflectivity) using the '*j-curve*' analysis presented by van der Neut *et al.* (2015b). This method provides a solution that can be implemented regardless of the dimensionality of the seismic data, and therefore reduces systematic and subjective errors in the comparisons we make in the following sections.

5 GREEN'S FUNCTION ESTIMATION WITH A 2-D-SEISMIC PROFILE

5.1 In-plane reflections

All previous applications of Marchenko methods in geophysics (using both synthetic and real data) have used seismic data sets collected along a spatially linear acquisition geometry. This is a reasonable avenue of study as it is common to acquire seismic data along a line of sources and receivers where only one of the horizontal coordinates varies. However, with the exception of real data applications, these studies have also been limited to 2-D media. In this section we investigate Marchenko solutions when the acquisition geometry is linear but wave propagation is 3-D. The differences in the measured seismic responses are of the type defined in eqs (10) and (11) and illustrated in Fig. 2.

To test the impact of these differences we extract a linear-array data subset from the areal survey measured over the 3-D model given in Fig. 3(a), taken along the line $y = 1000$ m (see Fig. 3c). This provides a reflectivity profile collected with a constant y coordinate but with 3-D wave propagation and therefore 3-D Green's functions. This line was selected as it contains minimal out-of-plane reflections

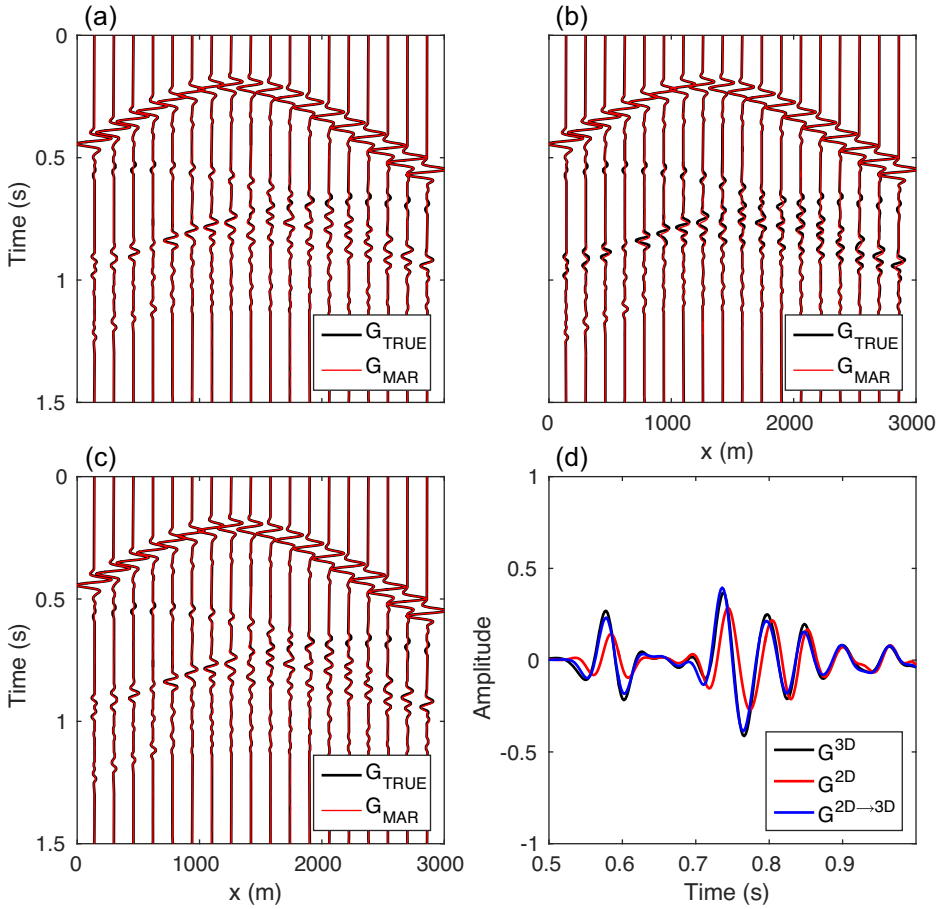

Figure 5. A comparison of the estimated Marchenko common receiver gathers (red) compared to the modelled receiver gathers (black). Panel (a) shows the fully 3-D Marchenko estimate, panel (b) shows the 2-D Marchenko estimate for waves propagating in three-dimensions, and panel (c) shows the dimensionally corrected 2-D Marchenko estimate. Panel (d) compares a single trace for each Marchenko estimate from source position (1292 m, 1000 m, 0 m). For display purposes a time dependent gain has been applied to all panels.

(we discuss the implications of those in more detail in the following section). We apply the 2-D equivalents of eqs (3)–(8) (Wapenaar *et al.* 2014) to this subsampled data set to calculate an estimate of the Green's functions between the surface sources and the same virtual receiver position as in the previous 3-D examples. We compare the solutions for 2-D and 3-D Marchenko methods applied to 3-D wavefields, as shown in Figs 5(b) and (a), respectively.

The results in Fig. 5(b) show calculation of the Green's functions. However the trace comparison highlights that there is a mismatch in phase between some components of the calculated and true solutions. This mismatch does not appear in the equivalent 3-D solution given in Fig. 5(a). It can therefore be assumed that the errors observed are due to the differences in acquisition geometries which impose the constraint that the 2-D Marchenko methods can not integrate over the second horizontal spatial dimension. A solution to overcome this problem is to apply a transform to the seismic data measured along a linear array but propagating in three-dimensions, to convert it into the 2-D equivalent data by implementing eq. (12). This modified data set can then be used as input into the 2-D Marchenko scheme and the result is then approximately equivalent to one propagating in two dimensions. For purposes of comparing it to the full 3-D solution it must therefore first be transferred back into its 3-D equivalent using eq. (13). The final estimate is displayed in Fig. 5(c).

Fig. 5(a) shows the fully 3-D result and can be viewed as a reference solution—the best result that can be achieved if 3-D seismic data is available over a dense areal array. The result in Fig. 5(b) uses a subsampled version of the 3-D data that is only recorded along a linear-array, thus forcing 2-D Marchenko methods to be applied which in turn produce a solution that contains phase errors. If we calculate the l_2-norm of the data misfit between the true and Marchenko result for both the reference solution and the result in Fig. 5(b) it increases by 60 per cent in the latter case. If we compare the l_2-norm of the data misfit between the reference solution and the dimensionally corrected result, shown in Fig. 5(c) (which uses the same input data as Fig. 5b), there is only a 4 per cent increase in the latter case. It is worth noting that the synthetic model in Fig. 3 has a constant velocity, therefore the amplitude versus offset variation is not as significant in Fig. 5 as it would be if the subsurface had an equivalent variable velocity structure. This means there is likely to be a larger mismatch in the gathers shown in Fig. 5 when there are variations in subsurface velocity (Mildner *et al.* 2019). Nevertheless, we have demonstrated how to accurately retrieve Marchenko solutions with 3-D wavefields when using 2-D seismic data: the data first needs to undergo dimensionality corrections. This method appears to be accurate in the case that there are minimal out-of-plane reflections in the data used.

5.2 Out-of-plane reflections

A significant motivation to use seismic data from areal arrays is their ability to discriminate reflections that occur outwith the vertical plane beneath any linear array and thus allow us to map 3-D geological structures accurately. In this section we investigate the implications of seismic data containing out-of-plane reflections on the solutions to the 2-D and 3-D Marchenko methods.

Consider a linear seismic array with a constant x coordinate of 1292 m (Fig. 3c) that is perpendicular to the line in the previous section. We use this dimensionally corrected data as input to the 2-D Marchenko method with results displayed in Fig. 6(b). For comparison we also use the data from the full areal array to construct the same virtual receiver gather with results shown in Fig. 6(a).

The results in Fig. 6 show that with a linear array spanning only part of the top boundary, the Marchenko method is not able to process out-of-plane reflections correctly. The final virtual receiver gather estimates are therefore inaccurate. However, when 3-D data is used for the same reconstruction the results are accurate.

6 MULTIDIMENSIONAL MARCHENKO IMAGING

One of the reasons Marchenko methods are of particular interest to Geophysicists is because of their applications in subsurface imaging. The Marchenko Green's functions estimates from eqs (3) and (4) can be used to produce seismic images with reduced multiple related contamination (Behura *et al.* 2014). Marchenko imaging operates similarly to other imaging algorithms such as RTM, by applying imaging conditions to the estimated subsurface wavefields to identify where seismic waves reflect. In this paper, as an example we use a cross-correlation imaging condition in which we calculate the zero-lag correlation coefficient of the upgoing Green's function (G^-) and the direct arrival estimate (T_d) at every desired image point $\mathbf{x}_i'$ to form the image I (Claerbout 1971; da Costa Filho *et al.* 2015):

$$I(\mathbf{x}_i') = \int_{\partial\mathbb{D}_0} \mathrm{d}\mathbf{x}_0'' \int_{-\infty}^{\infty} [G^-(\mathbf{x}_i', \mathbf{x}_0'', \omega) T_d(\mathbf{x}_i', \mathbf{x}_0'', \omega)^*] \, \mathrm{d}\omega. \tag{14}$$

This imaging condition essentially measures the similarity of the two input signals. We therefore rely on these two signals being similar when and only when the virtual receiver (image point) is on a subsurface interface, as would be the case if the downgoing direct-wave in T_d had caused the upgoing Green's functions G^- by reflection. However, given that the data we are using is frequency band-limited we expect reflectors to be identified within approximately half a wavelength of the true subsurface interface location. There are alternative imaging conditions that can be applied in Marchenko imaging which include deconvolution (Singh & Snieder 2017), multidimensional deconvolution (van der Neut *et al.* 2011) and imaging conditions that combine Marchenko imaging with reverse time migration at relatively little extra cost (da Costa Filho & Curtis 2016). Eq. (14) was chosen here because it is robust, cheap to compute, it has been shown to provide clean images in 2-D applications, and hence is a common choice amongst practitioners.

Applying eq. (14) to the redatumed Green's functions shown in Figs 5 and 6 gives four Marchenko images shown in Fig. 7 each of which is based on data taken from the same 3-D wavefields. The results in Figs 7(b) and (c), which use the data from Fig. 3(b) and the blue line from Fig. 3(c), respectively, identify all subsurface interfaces. The true locations of the interfaces are shown in Fig. 7(a). The input data for all of these images has undergone no pre-processing to remove internal multiples. Despite this there is limited evidence of false reflectors due to peg-leg multiples, which would be observed at ∼600 m if RTM was deployed for example. However, there are differences between the images presented in Fig. 7. The first and most significant is the error in interface depth imaging. To highlight this effect we picked the peak amplitude (which corresponds to the interface location) of the signal in each image and compare them in Fig. 7(a). This shows that the phase errors observed in Fig. 5(b) manifest themselves as depth errors of 16 m in the Marchenko image presented in Fig. 7(c). We have already demonstrated the accuracy of our dimensionality correction which would enable us to construct results similar to Fig. 7(b) with 2-D data. In Fig. 7(a) we have identified the true location of the subsurface interface within a margin of error of ±8 m, where the residual uncertainty corresponds to the image point spacing. In Figs 7 e and f we image an area of the subsurface perpendicular to the images in Figs 7(b) and (c) using the data from Fig. 3(b) and the red line from Fig. 3(c). Again, using the full 3-D seismic data we are able to obtain accurate images of the subsurface. However, when using a 2-D linear array of seismic data across the strike of the subsurface structure the resulting image is inaccurate. This is to be expected given the observed primary components of the wavefield originate from features out-of plane.

7 ACQUISITION GEOMETRIES

A limitation of all Marchenko methods is the requirement for dense source and receiver sampling along boundary $\partial\mathbb{D}_0$. This is particularly problematic in three dimensions given that the densely sampled area must span a surface rather than only a line. There is not a simple solution to this issue because the method we have implemented depends on constructive and destructive interference to calculate the Marchenko Green's functions; if traces required for either are missing due to limitations in the acquisition geometry then errors will occur. Therefore, for application to more practical or cost-efficient acquisition geometries an interpolation step may be required to densify data sampled in space. However, it is not clear what impact this would have on calculated Marchenko solutions as the interpolation method would have to be able to recreate data at points where the interference is critical. It could be that these issues are resolved by alternative methods for implementing the Marchenko method. Nevertheless this raises a further question: *what spatial resolution do Marchenko methods require to iterate to a solution?*

In Fig. 8, we have queried the relationship between the accuracy of Marchenko solutions and variable source–receiver spacing in a 2-D planar-layered medium (Fig. 8a). We have defined a virtual receiver position in the subsurface of the model at point $\mathbf{x}_i' = (1500, 1200)$, and calculated the Marchenko Green's functions (G_{MAR}) to this point, comparing them with the modelled Green's functions (G_{TRUE}). This comparison is made for a single trace between $\mathbf{x}_i'$ and a source position (1500,0) that is included within the array $\mathbf{x}_0''$. Our measure of accuracy is defined as:

$$Accuracy = \frac{1}{||G_{\mathrm{MAR}} - G_{\mathrm{TRUE}}||}, \tag{15}$$

where $||.||$ denotes the l_2-norm. The relationship between source–receiver spacing and Marchenko estimate accuracy (eq. 15) is likely to be dependent on both acquisition and subsurface properties. In Fig. 8(b) we have tested the dependency on dominant apparent wavelength (λ_A), which has been implemented by changing the dominant frequency of the Ricker wavelet source. It is also likely that there is a further dependency on structural dip in the subsurface, which we have not considered in this experiment. The results in Fig. 8 confirm

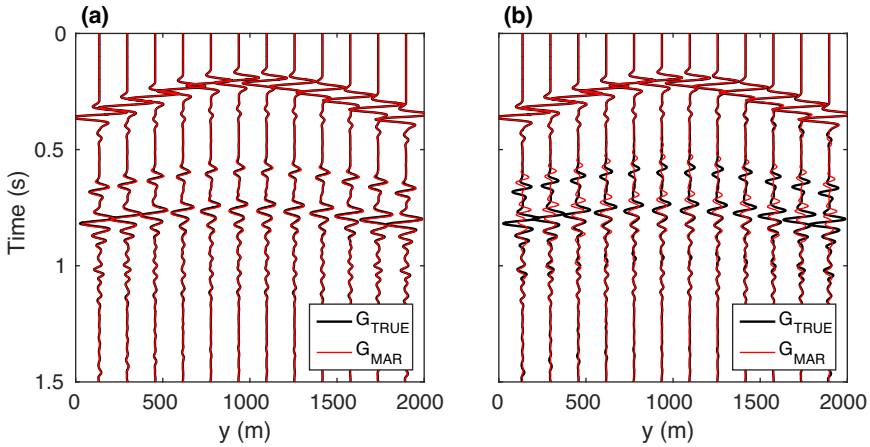

Figure 6. A comparison of two virtual receiver gathers constructed using Marchenko methods from seismic data recorded on a full areal array and a linear array where the data contain out-of-plane reflections. Panel (a) shows the gather constructed using the full areal survey. Panel (b) shows the gather constructed using only a seismic data subset from a linear array that contains out-of-plane reflections. In both panels the subsurface virtual receiver position is at (1292 m, 1000 m, 600 m) as shown in Fig. 3(a), and both the 2-D profile displayed and the data subset used in panel (b) have a constant x coordinate of 1292 m (Fig. 3c).

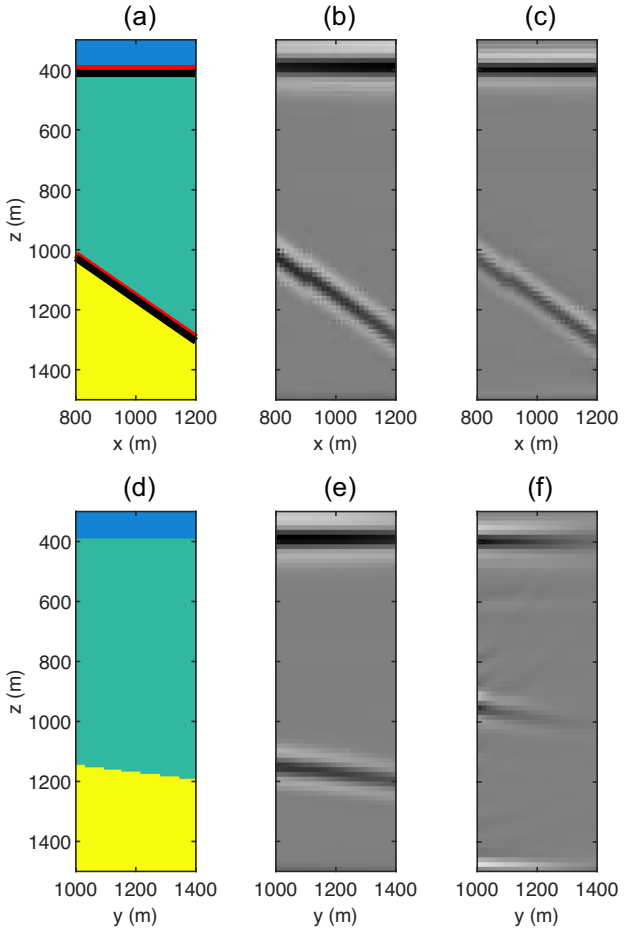

Figure 7. Panel (a) shows a 2-D slice ($y = 1000$ m) taken from the 3-D model in Fig. 3(a). Panel (b) is the 3-D Marchenko image created using the areal survey shown in Fig. 3(b). Panel (c) is a 2-D Marchenko image created using a seismic data set recorded on a linear array (the blue line in Fig. 3c) without dimensionality corrections. The red line in panel (a) corresponds to the peak amplitude in panel (b), likewise the black line corresponds to the peak amplitude in panel (c). Panel (d) shows a second 2-D slice ($x = 1000$), perpendicular to the line shown in panel (a). Panel (e) shows the 3-D Marchenko imaging result and panel (f) the 2-D Marchenko imaging result using the data set recorded on a linear array (the red line in Fig. 3c).

there is a dependency on dominant apparent wavelength, and from this graph we can extract an approximate empirical relationship for the successful application of Marchenko redatuming:

$$\Delta \mathbf{x}_0 \lessapprox \frac{\lambda_A}{4} \tag{16}$$

Typically for applications in seismic interferometry the Nyquist criterion is used to define the spatial sampling required for signal reconstruction (van Manen *et al.* 2006). However, the lowest frequency components of the signal will have a negligible contribution to the reconstructed signal, hence we have instead defined our empirical relationship in terms of dominant frequency. The results in Fig. 8 show that to retrieve accurate Marchenko solutions for the wavelengths tested the required source–receiver spacing can vary between maximum values of 19−38 m. Whilst this is only a 2-D experiment, if similar relationships hold in three dimensions these acquisition geometries are impractically dense. The solution going forward is therefore either to use 2-D data sets where dense acquisition geometries are possible, and as we have shown Green's functions using the Marchenko method can be accurately estimated. However, in areas of structural complexity where 3-D surveys are required, the iterative Marchenko method will require an interpolation step; the accuracy and implementation of this part of the workflow warrants further research.

8 DISCUSSION

8.1 Out-of-plane reflections

Given that we are implementing Marchenko methods as an iterative alogithm (as apposed to RTM which is not), this raises the question: *how* do out of plane reflections cause errors in Marchenko methods? The Marchenko method for Green's functions estimation presented in eqs (3)–(8) removes contamination due to multiples in the overburden by 'injecting' downgoing focusing functions along the top boundary $\partial \mathbb{D}_0$. These focusing functions are calculated using the traveltime and amplitude relationships present in the measured reflectivity (see van der Neut *et al.* 2015a). The 2-D Marchenko method assumes that all components of the measured reflectivity are caused by features in-plane. However, the out-of-plane events still contribute to the formation of focusing functions and this means

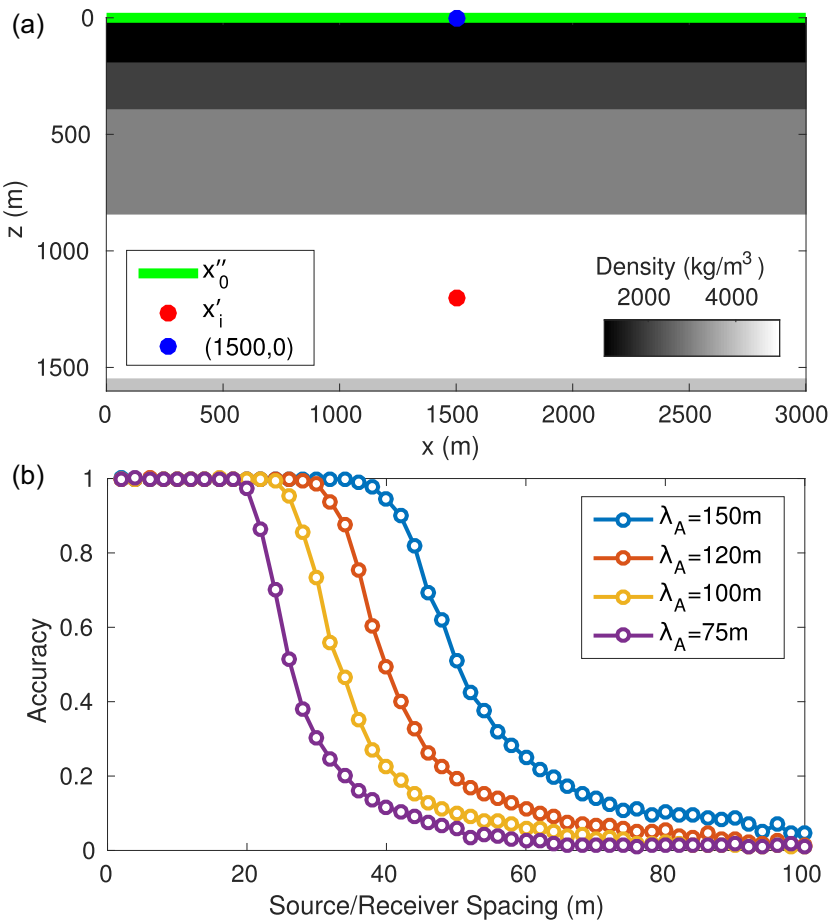

Figure 8. Fig. 10 A comparison of the accuracy of estimated Marchenko Green's functions with variable source–receiver spacing. Panel (a) shows the variable density constant velocity (1500 m s^{-1}) subsurface model, with the virtual receiver $\mathbf{x}_i'$, source array $\mathbf{x}_0''$ and the surface point (1500,0) from which the estimated Green's functions are calculated. Panel (b) compares the accuracy (eq. 15) of Marchenko estimates with increasing receiver spacings, these are shown to have a dependence on apparent dominant wavelength (λ_A) which are represented by the variable colours.

that the focusing functions will not be consistent, so the signal 'injected' at the surface will not accurately destructively interfere with the internal multiples within the seismic data. Therefore, the focusing functions will either not completely account for the internal multiples, or will add spurious multiples into the final result, both of which would cause the focus at $\mathbf{x}_i'$ to be imperfect. This would cause the Marchenko methods to produce inaccurate Green's function estimates. To demonstrate this in Fig. 9 we compare the imaging results from Fig. 7(f) with the image obtained using the initial estimates of the focusing functions, an imaging method equivalent to RTM (da Costa Filho & Curtis 2016).

In Fig. 9 we have highlighted two features in the Marchenko image (Fig. 9a) and the image produced using conventional methods (Fig. 9b). The first is the presence of a 'false' subsurface reflector indicated by the red arrow. This is present in both of the images which suggests the out of plane-reflectors are disrupting the focus and these events are not removed for the Green's function estimation. A second more concerning feature, highlighted by the blue arrow in Fig. 9(b), is the increase in coherent noise in the Marchenko imaging result. Again, this could be explained by the algorithm's inability to focus when out-of-plane reflections are included in the input data, the focusing energy is instead misplaced and causes additional artefacts to be superimposed on the resulting images.

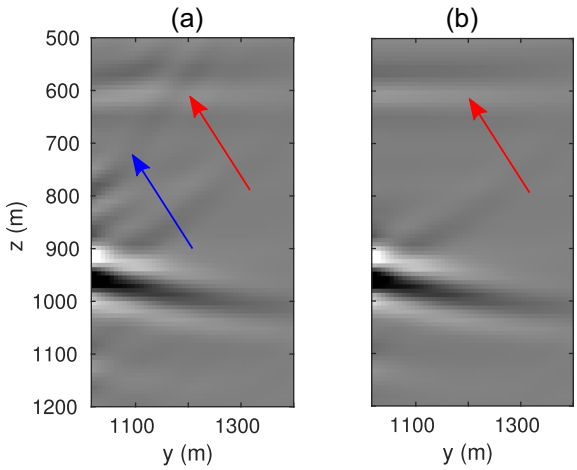

Figure 9. A comparison of (a) Marchenko imaging and (b) conventional imaging results created using seismic data collected along a linear seismic array (the red line in Fig. 3c). Highlighted by the red arrows in both images is a 'false reflector' created by internal multiples in the input seismic data. The blue arrows identifies artefects which are present only in the Marchenko imaging result. For comparison purposes the true model is given in Fig. 7(d).

Table 1. A comparison of the number of convolutions required for Marchenko Green's functions calculation with increasing dimensionality. Column two provides a formula for the calculation count and column three is an example based on the survey parameters used within this paper (Fig. 3b) with $n = 5$.

	Number of convolutions	Example
1-D	$2n + 3$	13
2-D	$(2n + 3)(nx^2)$	1.41×10^5
3-D	$(2n + 3)(nx^2 \times ny^2)$	4.56×10^8

8.2 Computational cost

Consider first the differences in storage requirements for Marchenko methods applied to 2-D and 3-D seismic data. There are three variables that impact the size of the seismic data set: the number of time samples per trace (N_t), the number of sources (N_s) and the number of receivers (N_r): the total number of time samples in a seismic data set is: $N_t \times N_s \times N_r$. If we assume that the number of sources is equal to the number of receivers (they are colocated) and that the number of sources in the y direction is equal to the number of sources in the x directions we can quantify the change in file size between two and three dimensions—this factor is $N_{s/r}^2$. For acquisition setups even with relatively few sources and receivers this scaling factor increases the data storage requirements by several orders of magnitude. In practice this can be reduced through survey design and data compression. This is a problem for implementation of any imaging algorithm in three dimensions (e.g. RTM), however, for the implementation of the Marchenko method defined in this paper we require the full reflection response (from every source to every receiver) to be convolved with the intermediate outputs (eqs 5–7) multiple times to calculate the Green's function for a single imaging point. Therefore due to the large file size the 3-D Marchenko methods require shared memory machines and parallelized algorithms to keep processing times reasonable.

It is also of interest to quantify how the number of calculations required to implement Marchenko methods scales with increasing dimensionality. The most computationally intensive parts of the algorithm (in higher dimensions) are the convolution steps. Therefore, in Table 1 we have calculated the number of convolutions required for the implementation of Marchenko methods in 1-D, 2-D and 3-D. Here n is the number of iterations, nx is the number of sources–receivers in the x direction, and ny is the number of sources–receivers in the y dimension. In Table 1 the number of convolutions $2n + 3$ is the number of times in the Marchenko workflow each input trace is convolved with each trace in the reflectivity. The second component of this equation (e.g. nx^2) is a function of the size of the reflectivity which therefore varies between dimensions. This term accounts for the number of convolutions between every source and every receiver, so its value is the size of the data squared. There are several orders of magnitude between the calculation count required in different dimensionalities, and because of this in the examples conducted herein the run-time of the algorithm for a single Green's function estimate varies from fractions of a second in lower dimensionalities to hours in higher dimensionalities.

9 CONCLUSION

In this paper, we have shown that Marchenko methods can be applied to seismic data from areal arrays (so-called 3-D seismic data) in order to image subsurface structures that are 3-D. However, if only linear seismic acquisition arrays are used, the reflectivity must first undergo amplitude and phase corrections to be consistent with the 2-D Marchenko equations which must be applied. These corrections result in significantly improved Green's function estimates. However, when out-of-plane reflections occur in the subsurface, 2-D Marchenko methods are unable to estimate Green's functions accurately. This is because the accuracy of the focusing functions is reduced so the advantages of the Marchenko method are compromised and the resulting images are less accurate than those produced using standard imaging methods. The minimum density of arrays required to implement the Marchenko methods is a receiver spacing of approximately $\lambda_A/4$ where λ_A is the dominant wavelength. This represents an impractical constraint in many real acquisition scenarios. Future work will require careful consideration of the mode of implementation and the associated computational costs of applying Marchenko methods in three dimensions.

ACKNOWLEDGEMENTS

The authors would like to thank Petrobras and Shell for their sponsorship of the International Centre for Carbonate Reservoirs (ICCR), and for permission to publish this work from the VSP project. We would also like to thank the fellow members of the ICCR and members of the Edinburgh Interferometry Project (EIP) for their numerous fruitful discussions. Finally, we would like to thank Patrick Elison and an anonymous reviewer for their comments which helped to improve this paper. The data within this paper were generated using the Madagascar open-source software package freely avaliable from www.ahay.org.

REFERENCES

Auer, L., Nuber, A.M., Greenhalgh, S.A., Maurer, H. & Marelli, S., 2013. A critical appraisal of asymptotic 3D-to-2D data transformation in full-waveform seismic crosshole tomography, *Geophysics,* **78**(6), R235–R247.

Baysal, E., Kosloff, D.D. & Sherwood, J.W., 1983. Reverse time migration, *Geophysics,* **48**(11), 1514–1524.

Behura, J., Wapenaar, K. & Snieder, R., 2014. Autofocus imaging: image reconstruction based on inverse scattering theory, *Geophysics,* **79**(3), A19–A26.

Bleistein, N., 1986. Two-and-one-half dimensional in-plane wave propagation, *Geophys. Prospect.,* **34**(5), 686–703.

Broggini, F., Snieder, R. & Wapenaar, K., 2012. Focusing the wavefield inside an unknown 1D medium: beyond seismic interferometry, *Geophysics,* **77**(5), A25–A28.

Claerbout, J.F., 1971. Toward a unified theory of reflector mapping, *Geophysics,* **36**(3), 467–481.

Cui, T., Becker, T.S., van Manen, D.-J., Rickett, J.E. & Vasconcelos, I., 2018a. Marchenko redatuming in a dissipative medium: numerical and experimental implementation, *Physical Review Applied,* **10**(4), 044022.

Cui, T., Vasconcelos, I., Manen, D.-J.V. & Wapenaar, K., 2018b. A tour of Marchenko redatuming: focusing the subsurface wavefield, *Leading Edge,* **37**(1), 67a1–67a6.

Curtis, A., Gerstoft, P., Sato, H., Snieder, R. & Wapenaar, K., 2006. Seismic interferometry–turning noise into signal, *Leading Edge,* **25**(9), 1082–1092.

da Costa Filho, C.A. & Curtis, A., 2016. Attenuating multiple-related imaging artifacts using combined imaging conditions, *Geophysics,* **81**(6), S469–S475.

da Costa Filho, C.A., Ravasi, M., Curtis, A. & Meles, G.A., 2014. Elastodynamic Green's function retrieval through single-sided Marchenko inverse scattering, *Phys. Rev. E,* **90**(6), 063201.

da Costa Filho, C.A., Ravasi, M. & Curtis, A., 2015. Elastic P-and S-wave autofocus imaging with primaries and internal multiples, *Geophysics,* **80**(5), S187–S202.

da Costa Filho, C.A., Tant, K., Curtis, A., Mulholland, A. & Moran, C.M., 2018. Using laboratory experiments to develop and test new [M]archenko and imaging methods, in *Proceedings of the SEG Technical Program Expanded Abstracts 2018,* pp. 4352–4356, Society of Exploration Geophysicists.

Galetti, E., Halliday, D. & Curtis, A., 2013. A simple and exact acoustic wavefield modeling code for data processing, imaging, and interferometry applications, *Geophysics,* **78**(6), F17–F27.

Jia, X., Guitton, A., Singh, S. & Snieder, R., 2017. Subsalt Marchenko imaging: a Gulf of Mexico example, in *Proceedings of the SEG Technical Program Expanded Abstracts 2017,* pp. 5588–5592, Society of Exploration Geophysicists.

Lomas, A. & Curtis, A., 2017. 3D seismic imaging using Marchenko methods, in *Proceedings of the AGU Fall Meeting Abstracts,* pp. NS31C–03.

Lomas, A. & Curtis, A., 2019. An introduction to Marchenko methods for imaging, *Geophysics,* **84**(2), 1MA–Z11.

Marchenko, V.A., 1955. On reconstruction of the potential energy from phases of the scattered waves, *Dokl. Akad. Nauk SSSR,* **104,** 695–698.

Mildner, C., Dukalski, M., Elison, P., De Vos, K., Broggini, F. & Robertsson, J., 2019. True amplitude-versus-offset Green's function retrieval using augmented Marchenko focusing, in *Proceedings of the 81st EAGE Conference and Exhibition 2019*.

Ravasi, M., Vasconcelos, I., Kritski, A., Curtis, A., Filho, C.A.D.C. & Meles, G.A., 2016. Target-oriented Marchenko imaging of a North Sea field, *Geophys. Suppl. Mon. Not. R. Astron. Soc.,* **205**(1), 99–104.

Rose, J.H., 2001. Single-sided focusing of the time-dependent Schrödinger equation, *Phys. Rev. A,* **65**(1), 012707.

Singh, S. & Snieder, R., 2017. Strategies for imaging with Marchenko-retrieved Greens functions, *Geophysics,* **82**(4), 1–68.

Singh, S., Snieder, R., Behura, J., van der Neut, J., Wapenaar, K. & Slob, E., 2015. Marchenko imaging: imaging with primaries, internal multiples, and free-surface multiples, *Geophysics,* **80**(5), S165–S174.

Singh, S., Snieder, R., van der Neut, J., Thorbecke, J., Slob, E. & Wapenaar, K., 2016. Accounting for free-surface multiples in Marchenko imaging, *Geophysics,* **82**(1), R19–R30.

Slob, E., Wapenaar, K., Broggini, F. & Snieder, R., 2014. Seismic reflector imaging using internal multiples with Marchenko-type equations, *Geophysics,* **79**(2), S63–S76.

Snieder, R., 2004a. Extracting the Green's function from the correlation of coda waves: a derivation based on stationary phase, *Phys. Rev. E,* **69**(4), 046610.

Snieder, R., 2004b. *A Guided Tour of Mathematical Methods,* Cambridge University Press.

Staring, M., Pereira, R., Douma, H., van der Neut, J. & Wapenaar, K., 2018. Source-receiver Marchenko redatuming on field data using an adaptive double-focusing method, *Geophysics,* **83**(6), 1–48.

Thorbecke, J., Slob, E., Brackenhoff, J., van der Neut, J. & Wapenaar, K., 2017. Implementation of the Marchenko method, *Geophysics,* **82**(6), 1–56.

van der Neut, J., Thorbecke, J., Mehta, K., Slob, E. & Wapenaar, K., 2011. Controlled-source interferometric redatuming by crosscorrelation and multidimensional deconvolution in elastic media, *Geophysics,* **76**(4), SA63–SA76.

van der Neut, J., Vasconcelos, I. & Wapenaar, K., 2015a. On Green's function retrieval by iterative substitution of the coupled Marchenko equations, *Geophys. J. Int.,* **203**(2), 792–813.

van der Neut, J., Wapenaar, K., Thorbecke, J. & Slob, E., 2015b. Practical challenges in adaptive Marchenko imaging, in *Proceedings of the SEG Technical Program Expanded Abstracts 2015,* pp. 4505–4509, Society of Exploration Geophysicists.

van der Neut, J., Wapenaar, K., Thorbecke, J., Slob, E. & Vasconcelos, I., 2015c. An illustration of adaptive Marchenko imaging, *Leading Edge,* **34**(7), 818–822.

van Manen, D.-J., Robertsson, J.O. & Curtis, A., 2005. Modeling of wave propagation in inhomogeneous media, *Phys. Rev. Lett.,* **94**(16), 164301.

van Manen, D.-J., Curtis, A. & Robertsson, J.O., 2006. Interferometric modeling of wave propagation in inhomogeneous elastic media using time reversal and reciprocity, *Geophysics,* **71**(4), SI47–SI60.

Wapenaar, C. & Grimbergen, J., 1996. Reciprocity theorems for one-way wavefields, *Geophys. J. Int.,* **127**(1), 169–177.

Wapenaar, K., 2014. Single-sided Marchenko focusing of compressional and shear waves, *Phys. Rev. E,* **90**(6), 063202.

Wapenaar, K. & Fokkema, J., 2006. Green's function representations for seismic interferometry, *Geophysics,* **71**(4), SI33–SI46.

Wapenaar, K., Broggini, F., Slob, E. & Snieder, R., 2013. Three-dimensional single-sided Marchenko inverse scattering, data-driven focusing, Green's function retrieval, and their mutual relations, *Phys. Rev. Lett.,* **110**(8), 084301.

Wapenaar, K., Thorbecke, J., van der Neut, J., Broggini, F., Slob, E. & Snieder, R., 2014. Marchenko imaging, *Geophysics,* **79**(3), WA39–WA57.

Wapenaar, K., Brackenhoff, J., Thorbecke, J., van der Neut, J., Slob, E. & Verschuur, E., 2018. Virtual acoustics in inhomogeneous media with single-sided access, *Scient. Rep.,* **8**(1), 2497.